nature structural & molecular biology

Structure of the ribosome-bound cricket paralysis virus IRES RNA

Martin Schüler[1], Sean R Connell[1], Aurelie Lescoute[2], Jan Giesebrecht[1], Marylena Dabrowski[1], Birgit Schroeer[1], Thorsten Mielke[3], Pawel A Penczek[4], Eric Westhof[2] & Christian M T Spahn[1]

Internal ribosome entry sites (IRESs) facilitate an alternative, end-independent pathway of translation initiation. A particular family of dicistroviral IRESs can assemble elongation-competent 80S ribosomal complexes in the absence of canonical initiation factors and initiator transfer RNA. We present here a cryo-EM reconstruction of a dicistroviral IRES bound to the 80S ribosome. The resolution of the cryo-EM reconstruction, in the subnanometer range, allowed the molecular structure of the complete IRES in its active, ribosome-bound state to be solved. The structure, harboring three pseudoknot-containing domains, each with a specific functional role, shows how defined elements of the IRES emerge from a compactly folded core and interact with the key ribosomal components that form the A, P and E sites, where tRNAs normally bind. Our results exemplify the molecular strategy for recruitment of an IRES and reveal the dynamic features necessary for internal initiation.

Initiation of protein synthesis is an essential phase of protein synthesis and a key regulatory step in gene expression[1,2]. In eukaryotes, the canonical 5′ cap–dependent pathway is facilitated and orchestrated by approximately 11 translation initiation factors. However, IRES RNAs can functionally substitute for initiation factors and facilitate the alternative pathway of internal initiation[3,4]. IRESs are present in 5′ untranslated regions (UTRs) of many viral RNAs and are efficient tools to hijack the translational apparatus of the host during viral infection. They are also used by a subset of cellular messenger RNAs—for example, several proto-oncogenes[3–5]. In this context, they act as regulatory tools and are used to initiate translation during cellular stress or other periods when overall global translation is compromised.

The molecular mechanisms of initiation by IRES RNAs are largely unknown. IRES RNAs fall into different classes that are distinguished by their structure and dependence on different sets of canonical initiation factors and IRES *trans*-acting factors[3–6]. The simplest mechanism of initiation is used by the intergenic IRESs of dicistroviruses, such as the cricket paralysis virus (CrPV). This family of IRESs does not require any initiation factor or even initiator tRNA in order to assemble elongation-competent 80S ribosomes[7–10]. According to biochemical studies, the IRES binds directly to the ribosomal 40S subunit and sets the translational reading frame by positioning the first codon into the ribosomal A site. This is highly unusual, because canonical initiation starts from the P site. Moreover, like the hepatitis C virus IRES[11], the CrPV IRES actively manipulates the conformation of the translational machinery, suggesting that the IRES acts like an RNA-based translation factor[12].

A detailed knowledge of the CrPV IRES structure, especially in the ribosome-bound state, is a prerequisite for understanding the mechanism of internal initiation without initiation factors. The low resolution of the previous cryo-EM maps limits analysis of the CrPV IRES architecture and precludes detailed molecular descriptions of interactions with the ribosome[12]. Therefore, we decided to improve the resolution of the cryo-EM map of the CrPV IRES–80S ribosome complex. To do so, we made use of the finding that the CrPV IRES is active not only in higher eukaryotes but also in yeast[13]. Yeast 80S ribosomes and wheat-germ 80S ribosomes have thus far proved to be better suited for high-resolution cryo-EM studies than mammalian 80S ribosomes[14,15]; indeed, we were able to obtain a cryo-EM structure of the CrPV IRES bound to the yeast 80S ribosome at a notably improved resolution of 7.3 Å. The resolution in the subnanometer range allowed *de novo* modeling of the complete CrPV IRES RNA. The resulting molecular model suggests different functional roles for the three pseudoknot-containing domains of the IRES and allows a molecular interpretation of the interactions of exposed elements of the IRES with ribosomal components located mainly at the A, P and E sites.

RESULTS

Cryo-EM reconstruction of the CrPV IRES–80S complex

After preparing CrPV IRES–80S ribosome complexes from *Saccharomyces cerevisiae*, the complexes were separated from unassociated subunits by sucrose-gradient centrifugation and used in cryo-EM experiments. For structural analysis, we collected an initial dataset

[1]Institut für Medizinische Physik und Biophysik, Charite-Universitätsmedizin Berlin, Ziegelstrasse 5-9, 10117-Berlin, Germany. [2]Architecture et Réactivité de l'ARN, Université Louis Pasteur, Institut de Biologie Moléculaire et Cellulaire, Centre National de la Recherche Scientifique, 15 rue R. Descartes, F-67084 Strasbourg, France. [3]UltraStrukturNetzwerk, Max Planck Institute for Molecular Genetics, Ihnestr. 73, 14195-Berlin, Germany. [4]The University of Texas-Houston Medical School, 6431 Fannin, Houston, Texas 77030, USA. Correspondence should be addressed to C.M.T.S. (christian.spahn@charite.de).

Received 20 September; accepted 31 October; published online 19 November 2006; doi:10.1038/nsmb1177

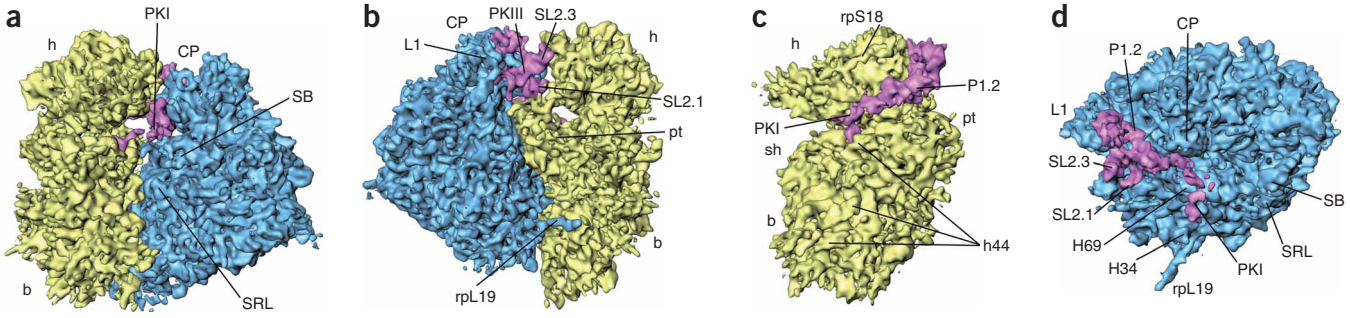

Figure 1 Cryo-EM map of the CrPV IRES RNA in complex with the yeast 80S ribosome. (**a**–**d**) The map is shown from the A site (**a**), from the L1 protuberance side (**b**), from the back of the 60S subunit with the 60S subunit removed (**c**) and from the top with the 40S subunit removed (**d**). Yellow, 40S subunit; blue, 60S subunit; magenta, CrPV IRES. Landmarks for the 40S subunit: b, body; h, head; pt, platform; sh, shoulder. Landmarks for the 60S subunit: CP, central protuberance; L1, L1 protuberance; SB, stalk base; SRL, sarcin-ricin loop. Also indicated: some prominent helices of the 18S rRNA (h44 in **c**) and the 25S rRNA (H34, H69 in **d**); the resolved α-helical density for rpS18 (**c**) and rpL19 (**b**,**d**); and some secondary structure elements of the CrPV IRES (see **Fig. 2**).

of 291,117 projections of individual ribosomal complexes derived from 341 micrographs. However, to account for conformational heterogeneity of the complexes, multireference classification techniques were used during structural refinement, and therefore only a subset of particles was used for the final reconstruction. The final reconstruction reached a resolution of 7.3 Å, according to the Fourier shell correlation curve using the 0.5 cutoff criterion (**Supplementary Fig. 1** online). In agreement with this resolution estimate, the grooves of the ribosomal RNA helices are easily distinguished, and α-helical secondary structure of ribosomal proteins is clearly resolved (**Fig. 1**). In good overall agreement with previous cryo-EM results, density for the CrPV IRES can be observed in the intersubunit space of the ribosome. Parts of the IRES density are not as well defined as the ribosomal density, indicating their inherent flexibility (**Fig. 1d**, PKI region). However, for the most part, the grooves of RNA helices are well defined, and density even for single-stranded RNA can be observed in some locations (**Fig. 2**; see below), allowing the sugar-phosphate backbone of the RNA to be traced.

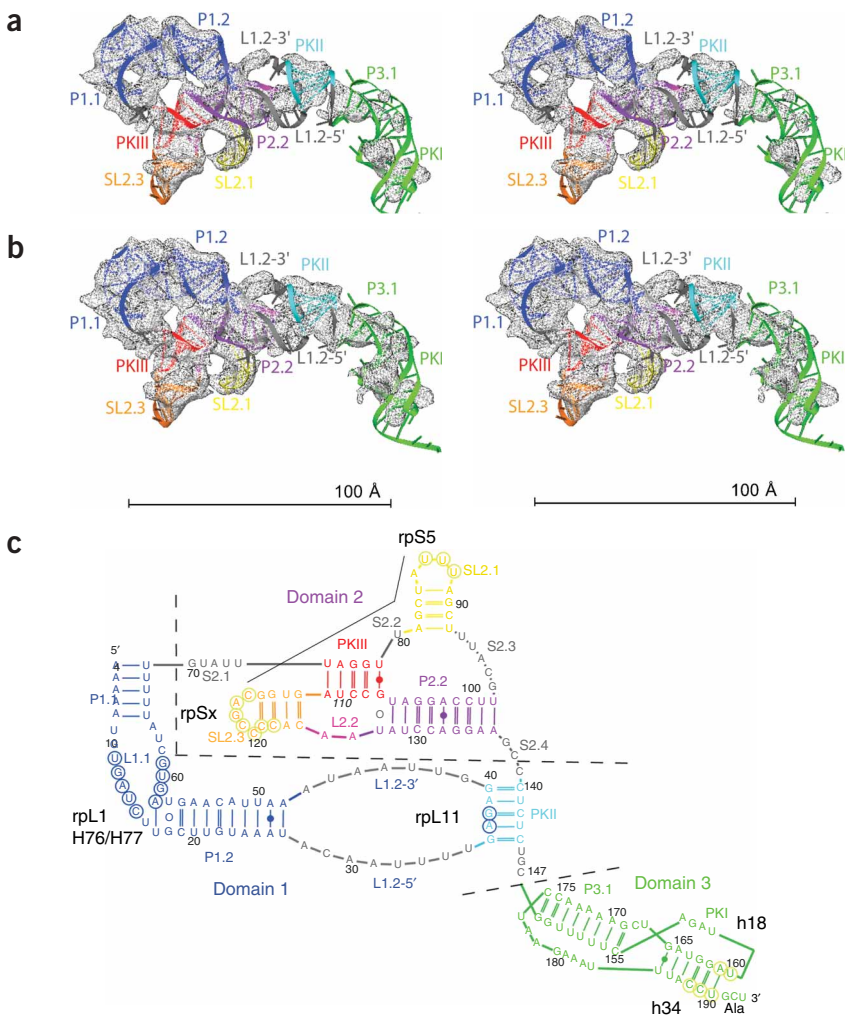

Figure 2 Structure of the CrPV IRES RNA. (**a**,**b**) Stereo view of the IRES molecular model, shown as a colored ribbon docked into the cryo-EM density (gray mesh), at two contour levels. (**c**) Secondary structure of the IRES[16–18]. Secondary structure elements are color-coded in the molecular model (**a**,**b**) and in the secondary structure diagram (**c**) and are labeled using the nomenclature of ref. 24. Dotted lines indicate separation of domains. IRES nucleotides that are likely candidates for interacting with the ribosome (see **Fig. 3**) are circled, and each likely ribosomal-component partner is indicated in the secondary structure diagram (**c**).

Molecular structure of the CrPV IRES RNA

At the present resolution, it is not possible to derive directly the identity of the helical RNA elements or their directionality, but the established secondary structure of the CrPV IRES[16–18] indicates the presence of three pseudoknots (PKI, PKII and PKIII) and establishes the length and connectivity of the helical elements (**Fig. 2c**). Additionally,

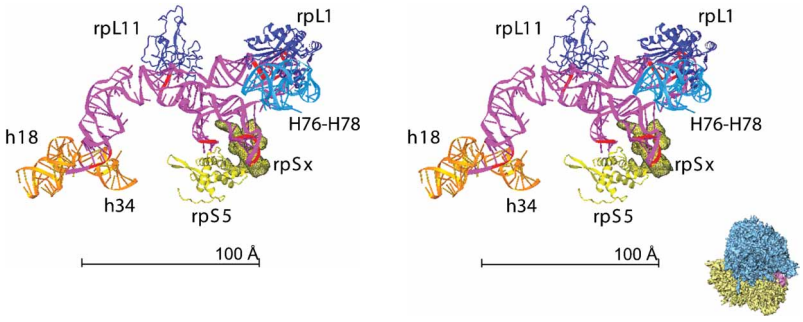

Figure 3 Molecular interactions of the CRPV IRES with the 80S ribosome. Stereo view of the IRES model (magenta ribbon) is shown, together with components of the 40S subunit (light green and orange ribbons; green wire mesh for the cryo-EM density of rpSx, a ribosomal protein with unknown identity) and the 60S subunit (blue ribbon) that appear to interact with the IRES. Positions of ribosomal components are derived from previous analysis[27]. A thumbnail is included as an orientation aid. A different orientation is shown in **Supplementary Fig. 5**. IRES nucleotides that are likely candidates for interacting with the ribosome are colored red and circled in the secondary structure diagram shown in **Figure 2c**.

the position and orientation of the PKI region is known from biochemical data, which dictates that the alanine start codon is placed in the decoding site of the 40S subunit[8,9,16,19]. Furthermore, several RNA pseudoknots have been solved to date by X-ray crystallography or NMR spectroscopy (for a review, see ref. 20). Therefore, the folding rules for many pseudoknots are understood and modeling of pseudoknots PKI and PKIII was guided by established structures.

Using this information as a starting point, it is possible to sequentially determine the identity and orientation of all the secondary structure elements in the cryo-EM density map (**Supplementary Notes** online). Moreover, density present in the cryo-EM map delineates plausible locations for the single-stranded regions, allowing meaningful three-dimensional modeling (**Fig. 2**). The possibility of connecting the helical fragments by single strands in a stereochemically correct manner is an important measure for the self-consistency of the derived model. Thus, we were able to interpret the entire cryo-EM density for the CrPV IRES RNA with a complete molecular model that contains 187 nucleotides (**Fig. 2**).

PKIII falls into a class of pseudoknots with only two single-stranded loop regions[20], such as the beet western yellow virus pseudoknot structure[21] (**Supplementary Fig. 2** online). The 5′ strand of helix P2.2 is continuous with the 3′ strand of helix PKIII (**Fig. 2c**), which leads to stacking of helices PKIII and P2.2 and positioning of strands S2.2 and S2.3 and stem-loop SL2.1 in the major/deep groove of P2.2. The two free adenines of loop L2.2 are in the minor/shallow groove of the PKIII helix (**Fig. 2**), where they can form A-minor contacts[22,23] with base pairs G77-C109 and G78-C108 of PKIII.

An important factor for maintaining the IRES structure appears to be helix P2.2, which contains an invariant noncanonical base pair between adenosines A102 and A132. Helix P2.2 appears to be stretched and not as tightly coiled as a canonical A-form RNA double helix, so it may deviate from the standard Watson-Crick geometry. In addition to the proposed stacking interactions with helix PKIII, potential non–Watson-Crick pairs may form in the major groove of P2.2 between the two central residues of S2.3 and the A•A and the following C-G pair (**Supplementary Fig. 3** online). Helix P2.2 may further be involved in interdomain interactions with domain 1. The densities corresponding to helices P1.2 and P2.2 are partially fused together, indicating tight helix-packing contacts around the non–Watson-Crick A•A pair. Below, the single strand L1.2-5′ runs through the minor groove of helix P2.2 (**Fig. 2**). Helix P1.1 and the internal loop L1.1, in domain 1, are solvent exposed and do not interact with domain 2.

Therefore, a compact core of the IRES appears to be formed by the stacked helices PKIII and P2.2, part of helix P1.2 and the single-stranded regions L1.2-5′, L2.2 and S2.3 (**Fig. 2**). Notably, when the IRES is folded in the presence of magnesium ions, this whole region becomes protected against hydroxyl radicals[24], which is in agreement with the present structural model of the IRES. In contrast to the pronounced interactions between domains 1 and 2, there appear to be no major interactions between domain 3 and the rest of the IRES, apart from the linker region connecting helices P3.1 and PKII (**Fig. 2**). Domain 3, which contains PKI, has previously been identified as an independently folding unit[8–10,16–19,24]. For homology modeling of this domain, we chose the human telomerase pseudoknot[25] as a template. It contains helices and linkers similar in length to those of the PK1 pseudoknot (**Supplementary Fig. 4** online).

Interactions between the CrPV IRES and the 80S ribosome

The IRES interacts in the intersubunit space with both the 40S and the 60S subunits[12]. The contacts can now be interpreted in molecular terms. A prominent feature of the CrPV IRES structure is the two stem-loops SL2.1 and SL2.3 of domain 2, which are exposed and contact the 40S subunit with their loops (**Fig. 3** and **Supplementary Fig. 5** online). SL2.1 interacts with ribosomal protein S5 (rpS5, also called S7p) close to the ribosomal E site and the exit channel for the mRNA[26]. SL2.3 interacts mainly with a neighboring protein of unknown identity, which lacks a homolog in the prokaryotic crystal structure[27]. Additional contacts appear to be made with rpS5, albeit further away from the E site. The two stem-loops have been strongly implicated in 40S binding by biochemical experiments showing that (i) domain 2 alone can bind the 40S subunit[17], (ii) deletion mutations in the two stem-loops strongly reduce IRES function[16], and (iii) nucleotides in the stem-loops are protected from chemical modification by the 40S subunit[17].

Interactions between domain 1 of the CrPV IRES and the ribosome are confined to the 60S subunit (**Fig. 3** and **Supplementary Fig. 5**). Helix PKII interacts with rpL11 (also called L5p). The internal loop L1.1 interacts with rpL1 (also called L1p) and helices H76 and H77 of the 25S rRNA. Both ribosomal sites interact with the T loop of tRNAs,

Figure 4 Comparison of the CrPV IRES with the location of the A-, P- and E-site tRNAs. Shown is a stereo view of the CrPV IRES molecular model superposed on tRNA models. Cyan, yellow and purple, IRES domains 1, 2 and 3, respectively (see **Fig. 2**); blue, A-site tRNA; green, P-site tRNA; orange, E-site tRNA. The tRNA coordinates[26] were superposed on the P-site tRNA of the yeast 80S ribosome[27], which had the same orientation as the CrPV IRES complexes.

rpL11 in the P site and rpL1-H76-H77 in the E site. Domain 3, which does not contribute to the binding affinity of the IRES for the ribosome[16,17,24], does not appear to be in tight contact with the ribosome. However, close to the alanine codon of the IRES, interactions can be observed with helices h18 in the shoulder region and h34 in the head of the 40S subunit (**Fig. 3** and **Supplementary Fig. 5**). Notably, both helices have been implicated in interactions with the anticodon stem-loop of the A-site tRNA[26].

DISCUSSION

Several features are remarkable in the distribution of interactions between the 80S ribosome and the CrPV IRES. The contacts are organized so that distinct functional tasks for the three IRES domains are immediately obvious. Domain 2 interacts with the 40S subunit in the E-site region, domain 1 contributes to the interactions with the 60S subunit in the E- and P-site regions, and domain 3 is functionally important because it places the alanine start codon into the decoding region of the A site. Moreover, all the interaction sites are outside of the compactly folded core structure of the IRES RNA (**Figs. 2** and **3**, and **Supplementary Fig. 5**). Finally, partially fragmented cryo-EM density for the IRES in the vicinity of the L1 protuberance indicates flexibility, especially for helix P1.1. This flexibility may be meaningful, because P1.1 interacts with the L1 protuberance, which is known to be dynamic[15,26,28–30], and therefore P1.1 must accommodate these changes.

In previous cryo-EM structures of CrPV–40S subunit complexes, domain 3 strongly overlaps with the position of the A-site tRNA and to some extent withdraws upon 80S ribosome formation[12]. Similarly, in our present high-resolution cryo-EM structure of the yeast 80S ribosome, domain 3 is located mainly between the A and P sites (**Fig. 4**), and only the apical part (containing the alanine codon) overlaps with the anticodon stem-loop of the A-site tRNA. The weaker cryo-EM density corresponding to domain 3 (compare **Fig. 2a**,**b**) indicates that flexibility occurs in this element as well, which is corroborated by the fact that only a few contacts with the ribosome and the two other domains of the IRES are formed. During the decoding of the alanine codon, domain 3 has to move completely out of the A site, and this could be facilitated by the flexibility of domain 3 without necessarily disrupting the contacts of domains 2 and 3, which would stabilize the initiation complex. Thus, the observed dynamic behavior of the IRES may allow it to adopt the various conformations it must assume while guiding the internal initiation reaction. The architecture of the IRES appears to balance the need of the IRES to be spatially compact with the ability to undergo conformational change. It remains to be seen how the CrPV IRES changes structure and interactions during subsequent steps—that is, A-site occupation and translocation.

In conclusion, our analysis provides a structural foundation for understanding the mechanism of internal initiation by the CrPV IRES and related IRES RNAs. Moreover, we show that it is possible to derive a *de novo* molecular model of an RNA molecule using high-resolution cryo-EM in combination with biochemical data. Until now, molecular-level interpretation of cryo-EM maps was largely dependent on the use of structures derived by X-ray crystallography or NMR spectroscopy, although we note that the fold of the hepatitis B virus core protein has been suggested on the basis of a cryo-EM reconstruction at 7.4-Å resolution[31]. Promising methods are being developed to identify secondary structure elements in cryo-EM maps[32], and, in line with this development, the successful modeling of a complete IRES RNA based on a cryo-EM map proves that single-particle cryo-EM is on the way to becoming a technique capable of *de novo* structure determination.

METHODS

Preparation of IRES–80S ribosome complexes. Ribosomal 40S and 60S subunits from yeast were isolated by standard procedures, and CrPV IRES was produced by *in vitro* transcription. 80S ribosomes were assembled in the presence of IRES RNA and then purified using sucrose-gradient centrifugation (for details, see **Supplementary Methods** online).

Cryo-EM reconstruction and RNA modeling. The complex was flash-frozen and imaged under low-dose conditions using an FEI–POLARA G2 electron microscope. The resulting data were digitized and processed using SPIDER[33]. The IRES RNA was modeled using MANIP[34], which allows one to build RNA molecules *ab initio* or by homology on the basis of previously determined crystal structures and to stereochemically refine the constructed RNA assemblies. Blocks of RNA were first docked manually into the cryo-EM density map using O[35]. The docking was supported by a cross-correlation–based search using SPIDER. The model was then manually and automatically refined using MANIP. This iterative process was repeated several times. Further information is provided in **Supplementary Methods**.

Accession codes. Protein Data Bank: coordinates have been deposited with accession code 2NOQ. Electron Microscopy Database: the cryo-EM map has been deposited with accession code EMD-1285.

Note: Supplementary information is available on the Nature Structural & Molecular Biology Website.

ACKNOWLEDGMENTS

This work was supported by a grant from the VolkswagenStiftung (to C.M.T.S.), by US National Institutes of Health grant R01 GM60635 (to P.A.P.), by the sixth EU framework program 3DEM and by the European Union and Senatsverwaltung für Wissenschaft, Forschung und Kultur Berlin (UltraStructureNetwork and Anwenderzentrum). S.R.C. was supported with a grant from the Alexander von Humboldt Stiftung.

COMPETING INTERESTS STATEMENT

The authors declare that they have no competing financial interests.

Published online at http://www.nature.com/nsmb/
Reprints and permissions information is available online at http://npg.nature.com/reprintsandpermissions/

1. Sonenberg, N. & Dever, T.E. Eukaryotic translation initiation factors and regulators. *Curr. Opin. Struct. Biol.* **13**, 56–63 (2003).
2. Dever, T.E. Gene-specific regulation by general translation factors. *Cell* **108**, 545–556 (2002).
3. Hellen, C.U. & Sarnow, P. Internal ribosome entry sites in eukaryotic mRNA molecules. *Genes Dev.* **15**, 1593–1612 (2001).
4. Vagner, S., Galy, B. & Pyronnet, S. Irresistible IRES: attracting the translation machinery to internal ribosome entry sites. *EMBO Rep.* **2**, 893–898 (2001).
5. Stoneley, M. & Willis, A.E. Cellular internal ribosome entry segments: structures, trans-acting factors and regulation of gene expression. *Oncogene* **23**, 3200–3207 (2004).
6. Jackson, R.J. Alternative mechanisms of initiating translation of mammalian mRNAs. *Biochem. Soc. Trans.* **33**, 1231–1241 (2005).
7. Sasaki, J. & Nakashima, N. Methionine-independent initiation of translation in the capsid protein of an insect RNA virus. *Proc. Natl. Acad. Sci. USA* **97**, 1512–1515 (2000).
8. Pestova, T.V. & Hellen, C.U. Translation elongation after assembly of ribosomes on the Cricket paralysis virus internal ribosomal entry site without initiation factors or initiator tRNA. *Genes Dev.* **17**, 181–186 (2003).
9. Wilson, J.E., Pestova, T.V., Hellen, C.U. & Sarnow, P. Initiation of protein synthesis from the A site of the ribosome. *Cell* **102**, 511–520 (2000).
10. Jan, E., Goss Kinzy, T. & Sarnow, P. Divergent tRNA-like element supports initiation, elongation and termination of protein biosynthesis. *Proc. Natl. Acad. Sci. USA* **100**, 15410–15415 (2003).
11. Spahn, C.M.T. *et al.* Hepatitis C virus IRES RNA-induced changes in the conformation of the 40S ribosomal subunit. *Science* **291**, 1962 (2001).
12. Spahn, C.M. *et al.* Cryo-EM visualization of a viral internal ribosome entry site bound to human ribosomes: the IRES functions as an RNA-based translation factor. *Cell* **118**, 465–475 (2004).

13. Thompson, S.R., Gulyas, K.D. & Sarnow, P. Internal initiation in *Saccharomyces cerevisiae* mediated by an initiator tRNA/eIF2-independent internal ribosome entry site element. *Proc. Natl. Acad. Sci. USA* **98**, 12972–12977 (2001).
14. Halic, M., Becker, T., Frank, J., Spahn, C.M. & Beckmann, R. Localization and dynamic behavior of ribosomal protein L30e. *Nat. Struct. Mol. Biol.* **12**, 467–468 (2005).
15. Spahn, C.M. *et al.* Domain movements of elongation factor eEF2 and the eukaryotic 80S ribosome facilitate tRNA translocation. *EMBO J.* **23**, 1008–1019 (2004).
16. Jan, E. & Sarnow, P. Factorless ribosome assembly on the internal ribosome entry site of cricket paralysis virus. *J. Mol. Biol.* **324**, 889–902 (2002).
17. Nishiyama, T. *et al.* Structural elements in the internal ribosome entry site of *Plautia stali* intestine virus responsible for binding with ribosomes. *Nucleic Acids Res.* **31**, 2434–2442 (2003).
18. Kanamori, Y. & Nakashima, N. A tertiary structure model of the internal ribosome entry site (IRES) for methionine-independent initiation of translation. *RNA* **7**, 266–274 (2001).
19. Pestova, T.V., Lomakin, I.B. & Hellen, C.U. Position of the CrPV IRES on the 40S subunit and factor dependence of IRES/80S ribosome assembly. *EMBO Rep.* **5**, 906–913 (2004).
20. Hilbers, C.W., Michiels, P.J. & Heus, H.A. New developments in structure determination of pseudoknots. *Biopolymers* **48**, 137–153 (1998).
21. Su, L., Chen, L., Egli, M., Berger, J.M. & Rich, A. Minor groove RNA triplex in the crystal structure of a ribosomal frameshifting viral pseudoknot. *Nat. Struct. Biol.* **6**, 285–292 (1999).
22. Battle, D.J. & Doudna, J.A. Specificity of RNA-RNA helix recognition. *Proc. Natl. Acad. Sci. USA* **99**, 11676–11681 (2002).
23. Nissen, P., Ippolito, J.A., Ban, N., Moore, P.B. & Steitz, T.A. RNA tertiary interactions in the large ribosomal subunit: the A-minor motif. *Proc. Natl. Acad. Sci. USA* **98**, 4899–4903 (2001).
24. Costantino, D. & Kieft, J.S. A preformed compact ribosome-binding domain in the cricket paralysis-like virus IRES RNAs. *RNA* **11**, 332–343 (2005).
25. Theimer, C.A., Blois, C.A. & Feigon, J. Structure of the human telomerase RNA pseudoknot reveals conserved tertiary interactions essential for function. *Mol. Cell* **17**, 671–682 (2005).
26. Yusupov, M.M. *et al.* Crystal structure of the ribosome at 5.5 Å resolution. *Science* **292**, 883–896 (2001).
27. Spahn, C.M.T. *et al.* Structure of the 80S ribosome from *Saccharomyces cerevisiae*—tRNA-ribosome and subunit-subunit interactions. *Cell* **107**, 373–386 (2001).
28. Harms, J. *et al.* High resolution structure of the large ribosomal subunit from a mesophilic eubacterium. *Cell* **107**, 679–688 (2001).
29. Valle, M. *et al.* Locking and unlocking of ribosomal motions. *Cell* **114**, 123–134 (2003).
30. Ban, N., Nissen, P., Hansen, J., Moore, P.B. & Steitz, T.A. The complete atomic structure of the large ribosomal subunit at 2.4 Å resolution. *Science* **289**, 905–920 (2000).
31. Bottcher, B., Wynne, S.A. & Crowther, R.A. Determination of the fold of the core protein of hepatitis B virus by electron cryomicroscopy. *Nature* **386**, 88–91 (1997).
32. Chiu, W., Baker, M.L., Jiang, W., Dougherty, M. & Schmid, M.F. Electron cryomicroscopy of biological machines at subnanometer resolution. *Structure* **13**, 363–372 (2005).
33. Frank, J. *et al.* SPIDER and WEB: processing and visualization of images in 3D electron microscopy and related fields. *J. Struct. Biol.* **116**, 190–199 (1996).
34. Massire, C. & Westhof, E. MANIP: an interactive tool for modelling RNA. *J. Mol. Graph. Model.* **16**, 197–205 255–7 (1998).
35. Jones, T.A. & Kjeldgaard, M. Electron density map interpretation. *Methods Enzymol.* **277B**, 173–207 (1997).